Supplementary Information on

Efficient triplet-triplet annihilation upconversion in binary crystalline solids fabricated by solution casting operating in air

Kenji Kamada[1,2*], Yusuke Sakagami[1,2], Toshiko Mizokuro[1], Yutaka Fujiwara[3], Kenji Kobayashi[3*], Kaishi Narushima[4], Shuzo Hirata[4], Martin Vacha[4]

[1]IMFRI, National Institute of Advanced Industrial Science and Technology (AIST), 1-8-31 Midorigaoka, Ikeda, Osaka 563-8577, Japan
[2]Department of Chemistry, School of Science and Technology Kwansei Gakuin University, Sanda, Hyogo 669-1337, Japan
[3]Department of Chemistry, Faculty of Science, Shizuoka University, 836 Ohya, Suruga-ku, Shizuoka 422-8529, Japan
[4]Department of Organic and Polymeric Materials, Tokyo Institute of Technology, Ookayama 2-12-1-S8, Meguro-ku, Tokyo 152-8552, Japan
** e-mail: k.kamada@aist.go.jp, kobayashi.kenji.a@shizuoka.ac.jp*

CONTENTS

Theory

S1. Theory for the excitation intensity dependence

Experimental

S2. Sample preparation
S3. General description on the optical microscope setup for emission and absorption measurements
S4. Position and size of the detection area of emission
S5. Estimation of excitation intensity under the microscope
S6. Measurements of excitation-intensity-dependence of the UC emission under the microscope
S7. Correction of the emission spectrum through the microscope optics
S8. Reference sample for QY measurement
S9. Determination of UC-QY of individual crystalline particles
S10. Preparation of the PtOEP-nanocrystal dispersed aqueous solution by the precipitation method
S11. High-resolution microscopic spectrograph.
S12. The UC-QY measurement using an integration sphere
S13. Transmission electron microscope (TEM) observation

Supplemental Data

S14. Absorption and emission spectra of the compounds used
S15. Polarized microscope observation of PtOEP:DPA cast sample
S16. SEM image of crystalline particle of PtOEP:DPA
S17. UC emission decay and the triplet lifetime
S18. Data of excitation-intensity dependence of the UC emission
S19. UC quantum yield of the PtOEP:C7-sDPA sample with the molar ratio of 1:1000

References

Theory

S1. Theory for the excitation intensity dependence

The reaction scheme generally accepted for the triplet-triplet annihilation (TTA) upconversion (UC) is following with the sensitizer (S) and emitter (E) as,

$^1S + h\nu_{ex}$	$\rightarrow$	$^1S^*$	: Absorption
$^1S^*$	$\rightarrow$	$^1S\ (+ h\nu_1)$	: Unimolecular singlet deexcitation
$^1S^*$	$\rightarrow$	$^3S^*$	: Intersystem crossing (ISC)
$^3S^*$	$\rightarrow$	$^1S\ (+ h\nu_2)$	: Unimolecular triplet deexcitation
$^3S^* + {}^1E$	$\rightarrow$	$^1S + {}^3E^*$	: Triplet-triplet energy transfer (TET)
$^3E^*$	$\rightarrow$	$^1E\ (+ h\nu_3)$	: Unimolecular triplet deexcitation
$^3E^* + {}^3E^*$	$\rightarrow$	$^1E^* + {}^1E$	: Triplet-triplet annihilation (TTA)
$^1E^*$	$\rightarrow$	$^1E\ (+ h\nu_{em})$	: Unimolecular singlet deexcitation

where the unimolecular deexcitations include radiative and nonradiative ones, $h\nu_{ex}$ is the incident photon, and $h\nu_1$, $h\nu_2$, $h\nu_3$, and $h\nu_{em}$ are the emitting photons of fluorescence and phosphorescence of the sensitizer, and phosphorescence and fluorescence of the emitter, respectively. The emission from the excited singlet emitter ($^1E^*$) in the last step is delayed fluorescence and that is the upconverted emission ($h\nu_{em}$).

With this model, the UC quantum efficiency (QY) of TTA-UC was described, as,[1]

$$\Theta = 1 + \frac{1 - \sqrt{1 + 2\Lambda}}{\Lambda} \qquad \text{(S1)}$$

with two dimensionless parameters,

$$\Theta \equiv \frac{\Phi_{UC}}{\phi_F \varphi_{TTA}} \qquad \text{(S2)}$$

and

$$\Lambda \equiv 4 k_{TTA} k_{TE}^{-2} N_{ex}\,; \qquad \text{(S3)}$$

the former is the normalized UC-QY ($0 \le \Theta \le 1$) where the ISC and TET QYs are assumed to be unity and the latter is the normalized excitation rate. Here Φ_{UC} is the UC-QY, ϕ_F is fluorescence (FL) QY of the emitter molecule, φ_{TTA} is the branching ratio to generate the excited singlet in the TTA process, k_{TTA} is the bimolecular rate constant of the TTA process, k_{TE} is the unimolecular deexcitation rate constant of the

emitter, and N_{ex} is the excitation rare (in Ms^{-1}).

Since the UC emission intensity I_{UC} is proportional to Φ_{UC} and the excitation light intensity I_{ex}, (i.e. $I_{UC} \propto \Phi_{UC} I_{ex}$), eq. 1 in the main text was obtained by putting eq. S2 into eq. S1 and this proportionality. The proportionality constant *K* contains $\phi_F \varphi_{TTA}$ and other constants such as the instrumental constant. Here we use the relation,

$$\Lambda = 2I_{ex}/I_{th} \qquad \text{(S4)}$$

because N_{ex} in eq. S3 is proportional to I_{ex} for a constant excitation area and Λ can be regarded as *normalized excitation intensity*. I_{th} means *threshold excitation intensity* and the reason is explained as follows. Here we define I_{th} as *the excitation intensity at which the excitation intensity dependence of the UC emission changes from quadratic to linear* as in many papers. In this definition, I_{th} is obtained as the excitation intensity at the crossing point of the extrapolated lines from the weak excitation (slope = 2) and strong excitation (slope = 1) regions in double logarithmic plot of I_{UC} versus Λ (Fig. S1, left). This definition is directly converted with Θ and Λ, i.e. the excitation intensity at the crossing point of the tangent line at the zero excitation (the weak excitation limit) and the $\Theta = 1$ line (the strong excitation limit) with eq. S1 because the order of Θ on Λ is lower by one order than that of I_{UC} [2-4] (Fig. S1, right). The differential coefficient of eq. S1 at the zero-excitation limit is,

$$\lim_{\Lambda \to 0}\left[\frac{d\Theta}{d\Lambda}\right] = \lim_{\Lambda \to 0}\left[\frac{d}{d\Lambda}\left(1 + \frac{1-\sqrt{1+2\Lambda}}{\Lambda}\right)\right] = \frac{1}{2}. \qquad \text{(S5)}$$

Thus, the normalized excitation intensity at the crossing point of the tangent line ($\Theta = \frac{1}{2}\Lambda$) and the saturation asymptotic line ($\Theta = 1$) is

$$\Lambda = 2. \qquad \text{(S6)}$$

The definition of eq. S4 gives $\Lambda = 2$ at $I_{ex} = I_{th}$, therefore I_{th} gives the excitation light intensity at the crossing point and satisfies the definition of the threshold excitation intensity.

Eqs. S1 and S6 immediately give $\Theta = 1 + \left(1-\sqrt{5}\right)\Big/2 \approx 0.382$ at $I_{ex} = I_{th}$. On the other hand, $\Theta = \frac{1}{2}$ is obtained when $I_{ex} = 2I_{th}$ corresponding to $\Lambda = 4$. We define this intensity as $I_{1/2}$ to distinguish from I_{th}. Monguzzi et al. defines as "I_{th} as at which $\phi_{TTA} = 0.5$" in their paper[3] where their ϕ_{TTA} correspond to Θ here, so their "I_{th}"

correspond to our $I_{1/2}$ as shown in above.

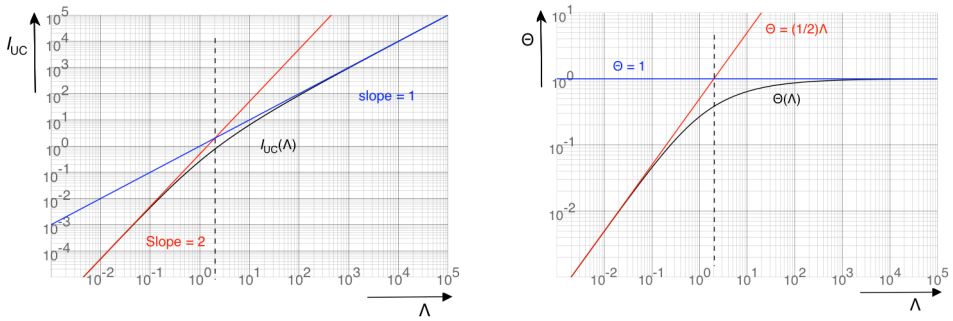

Fig. S1. Plot of the normalized excitation intensity(Λ)-dependence. Left: the UC emission intensity (I_{th}, arbitrary scale). Right: the normalized upconversion quantum yiled (Θ). The intensity at the crossing point is shown with dashed line.

Experimental

S2. Sample preparation.

Pt-octaethylporphyrin (PtOEP) and 9,10-diphenyl anthracene (DPA, purified by sublimation, >99.0%) was purchased from Sigma-Aldrich and Tokyo Kasei, respectively, and were used without further purification. C7-sDPA was synthesized according to the reported protocol.[5] DPA or C7-sDPA was dissolved in the tetrahydrofuran solution of PtOEP (THF, spectroscopic grade). The concentration of the sensitizer and emitter was [PtOEP] : [DPA] = 143 μM : 143 mM and [PtOEP] : [C7-sDPA] = 29 μM : 21 mM (or 21 μM : 21 mM for the data presented in Fig. S12). These concentrations of the emitters are saturated concentration in THF at the room temperature (23 °C). All solutions were prepared in ambient conditions. The mixed solution (~10 μl) was dropped on microscopic slide glass and dried in ambient conditions to obtain the cast samples. For the measurement of UC-QY under different atmosphere, a cover glass was placed over the sample with spacer (80 μm) and then sealed with UV curable adhesive (Norland optical adhesive #61). During UV irradiation for sealing, the sample area was masked to avoid possible photodamage. For the Ar-atmosphere samples, this procedure was performed in a globe box filled with Ar (>99.998%).

S3. General description on the optical microscope setup for emission and absorption measurements

An optical microscope (*Olympus BX50*) with 20x objective lens (NA=0.50) was used as the platform for the emission and absorption spectrum measurements. Continuous wave (cw) laser beam from a solid-state green laser (*Thorlabs CPS532* laser diode module or *Coherent Verdi,* depending on experiments) centered at 532 nm (spectral width 8 nm in FWHM) was attenuated by neutral density (ND) filter and steered to the microscope. No residual emission at the shorter wavelengths than the laser line was confirmed by monitoring the laser output spectrum and also by putting a short-cut filter in the excitation path. A part of the input beam picked by a beam splitter was used to monitor fluctuation of the laser power by an optical power meter (*Melles-Griot Universal Optical Power Meter* with Si detector head) during the measurements. The irradiation power was continuously varied by computer-controlled variable ND filer in the optical path. The laser beam was reflected by a half mirror mounted in a fluorescence cube of the microscope and illuminated the sample through an objective lens (20x, NA 0.5). Excitation power at the sample surface was measured by a calibrated microscope photodiode power sensor (*Thorlabs S170C*) connected to an optical power meter (*Thorlabs PM200*). The proportionality between the excitation power at the sample position and the laser power monitor was confirmed before usage. Fresnel reflection loss of the cover glass (~4%) was neglected because difference among the particles was much larger. The backward emission from the sample was collected by the same objective lens and led to the output port of the microscope through the same fluorescence cube.

A notch filter (centered at 532 nm, bandwidth 27 nm, OD 4) was placed at the detection side of the fluorescence cube. Through a multimode optical fiber (core diameter 400 μm, NA 0.48) placed at the imaging plane after the output port, the emission was detected by a fiber spectrometer (*Ocean Optics USB2000-FLG*). The detecting position was monitored by a CCD camera equipped to another output port the microscope.

On the measurements of UC emission, any artifact caused by the possible overtone of the lasers was confirmed to negligible by placing a shortcut filter (HOYA Y44) in the excitation path.

S4. Position and size of the detection area of emission

The position and size of the detection area of emission was checked by the knife-edge method. A sharp-edge aluminum mask fixed on slide glass was used to cut the illumination beam. By changing the position of the mask, the transmission light from the microscope illumination was detected. A CCD camera attached to the microscope monitored the edge position of the mask. This operation was repeated for *x*- and *y*-axis. The center of the detection area was determined as the position where the 50% transmission was obtained. The size was obtained as the full width at half maximum of derivative of the transmission curve as function of the mask position. The position of detection was located at the center of the excitation beam and the diameter of the detection area was 20 μm.

S5. Estimation of excitation intensity under the microscope

Radius of the excitation beam was determined by observing the fluorescence image of rhodamine 101 solution film in ethanol-glycerin (1:9 in volume) sandwiched between the glass plates. Curve fitting with two-dimensional Gaussian function to the recoded fluorescence image gave the $1/e^2$- radius of 95.8 μm (*x*-axis) and 108.1 μm (*y*-axis) for the case of *Verdi*. The beam was slightly elliptical, so the average of the radii (102.0 μm) was used for to calculate the intensity. With this radius of 102 μm, the average excitation intensity at the sample surface was determined to be 3.06 W/cm^2 for the excitation power of 1.0 mW. However, radius of the detection area (10 μm in radius, Section S4) was much smaller than that of this excitation area. Thus, the local intensity at the detection area should be considered as the real excitation intensity. The local intensity can be estimated by taking account of the Gaussian profile of the beam. The radial (*r*) distribution of the optical intensity is,[6]

$$I(r) = I_0 e^{-2r^2/w^2} \tag{S7}$$

where w is the $1/e^2$-radius and I_0 is the on-axis intensity (at $r = 0$), which has the relation with the average intensity I_{av} as

$$I_0 = 2\frac{P}{\pi w^2} = 2I_{av} \tag{S8}$$

with the beam power P. The excitation intensity of the detection area (r <10 μm) was

calculated to be 0.98~1.0 times of I_0 from eq. S7. Thus, the excitation intensity of the detection area was estimated to be $0.98 \times 2I_{av} = 0.98 \times 2 \times 3.06$ W/cm^2 = 6.0 W/cm^2 for P = 1 mW. For the case of the laser diode module, the same procedure gives 4.0 W/cm^2 for P = 0.9 mW input. *Verdi* was used for the excitation-intensity-dependence and UC-QY measurements because of the high stability in the intensity. The laser diode module was used to acquire the emission images and the spectra.

The change of the excitation intensity along the depth (focus) direction was also checked. Change of the radius of the excitation beam was <0.5% for the change of the focus of ±10 μm. Thus the intensity was regarded as constant for the depth of 20 μm, which is thinner than the thickness of the crystalline particles studied (<15 μm).

S6. Measurements of excitation-intensity-dependence of the UC emission under the microscope

The measurements of excitation-intensity-dependence of the UC emission intensity were carried out by using the setup mentioned above. The excitation intensity was varied by a computer-controlled variable ND filter with ordinary ND filters to change the intensity ranges. The excitation intensity was increased from the minimum to the maximum and then reduced back to the minimum for each intensity range. The data was acquired for the UC emission (440–448 nm for DPA and 430–438 nm for C7-sDPA to cover the peak wavelengths) and the scattering of the excitation light (528–535 nm, through the notch filter) as relative excitation intensity. At the maximum power of each excitation intensity range, the optical power was measured at the sample position and used to scale the relative excitation intensity to the absolute one for the recorded date points. The data for all intensity ranges were plotted in one double logarithmic graph (as in Figs. S10–11) and analyzed by curve fitting with eq. 1 in the main text, to obtained the threshold excitation intensities.

S7. Correction of the emission spectrum through the microscope optics

The fiber spectrometer was spectrally corrected by using the calibration light source (*Ocean Optics LS-1-CAL*) including the optical fiber used. The fluorescence spectra measured by the fiber spectrometer for fluorescence samples emitting the wavelength of interest (400-600 nm) agreed with those measured by a spectrofluorimeter (*Hitachi F-4500*) independently calibrated. The transmission spectrum of the microscope optics

(objective lens, beam splitter, notch filter, and other focusing optics to the output port connecting to the optical fiber) was measured by using the same the calibration light source. The obtained transmission spectrum was used for the calculation of the UC-QY.

S8. Reference sample for QY measurement

The solution of rhodamine 101 (Rh101, Exciton Inc.) in ethylene glycol (EG, Sigma-Aldrich spectrometric grade) was selected for the reference material of the microscopic measurement of UC-QY because the fluorescence (FL) QY of Rh101 is known to insensitive to temperature[7] as well as to oxygen concentration. Nonvolatile feature of EG is convenient to avoid the concentration change during measurement especially for the liquid film sample sandwiched between glass plates. To obtain reliable value of absorbance (>0.01 at 532 nm) in this configuration, we choose the concentration as 100 μM. To determine the FL-QY of the Rh101/EG solution at this concentration, we performed the following stepwise procedure.

First, FL-QY of diluted solution (0.5 μM, absorbance 0.013 in 1-cm cuvette at the excitation wavelength of 525 nm) of Rh101/EG was determined by using Rh101/ethanol solution of the same concentration as reference by using the spectroflorimeter in the orthogonal geometry. The optical path lengths were set to be the same for both samples. With the reported value for Rh101/ethanol (FL-QY = 0.89),[8] the FL-QY of the 0.5-μM Rh101/EG solution was determined to 0.94 including the correction for the refractive indices.

Second, the concentration effect of Rh101/EG was checked in the range of 0.5-100 μM with the same spectroflorimeter but by detecting the surface emission from a triangular cuvette to reduce the effect of the penetration depth of the excitation light.[9] The obtained FL-QY decreased at the concentrations over 10 μM (Fig. S2) due to insufficient suppression of the penetration-depth effect for the high concentrations.

Third, for the high concentration range (from 3 to 100 μM), we performed the FL-QY measurements of the Rh101/EG liquid film sandwiched between the glass plates with 80-μm spacer by using the aforementioned microscope setup (i.e. in the backward configuration). The FL-QY was found to be almost constant (within 10%) for all concentrations (Fig. S2). Finally, the FL-QY of Rh101/EG at 100 μM was determined to

be 0.94. All measurements were carried out in aerated condition.

In a separate experiment, the FL-QY of this concentration (100 μM) of Rh101/EG was measured by an absolute photoluminescence quantum yields measurement system (*Hamamatu Photonics, C9920-02*) with the reabsorption calibration based on the reported method.[10] The obtained FL-QY was 0.92±0.03, which agreed with this stepwise determination procedure.

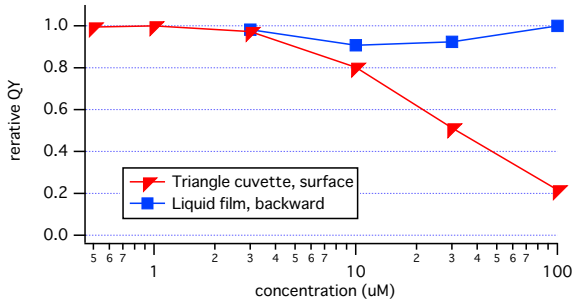

Fig. S2. Relative fluorescence quantum yield of rhodamine 101 solution in ethylene glycol with different concentration. The value at 0.5 μM was taken as unity for the measurement of surface emission with a triangle cuvette and the spetrofluorimeter (triangle). The results of the microscope measurement of backward emission with fiber spectrometer and liquid film (square) were scaled to the value with triangle cuvette at 3 μM.

S9. Determination of UC-QY of individual crystalline particles

The measurements of UC-QY were performed in the same manner as the fluorescence (FL) QY measurement under the microscope. To calculate the UC-QY, the following convention was used:

$$\Phi_S = 2\Phi_R \frac{F_S A_R P_R n_S^2}{F_R A_S P_S n_R^2} \qquad \text{(S9)}$$

Where Φ is QY, F is integrated intensity of the corrected emission spectrum, A is absorbance at the excitation wavelengths, P is excitation power, and n is refractive index. The suffixes of S and R mean *sample* and *reference*. The factor of 2 was used to express the full conversion as unity.

We selected a single crystalline particle of the sample under the microscope and positioned it so that the detection area overlapped the center of the particle. The excitation area, which is larger than the detection area as mentioned above, covered whole particle or large part of it, depending on the particle selected. We set the focus of

the microscope at the center between the bottom and top of the particle. All samples were covered by a cover glass with 80-μm spacer sealed with UV curable adhesive. For Ar-environment samples, the sealing was performed in a grove box filled with high purity Ar. The others were treated throughout in aerated condition.

The emission spectrum was measured at the excitation intensity of 6.0 W/cm^2 at the sample position. Fluctuation of the excitation power was always monitored and used for the correction. The spectral correction was carried out by the method described in Section S7. The reference (Rh101/EG, 100 μM, sandwiched between the same glass plates as used for the sample with the same thickness of spacer in order to keep the identical optical condition between the sample and reference; the FL-QY was 0.94 as described in Section S8) was measured under the same condition except changing the focal position so that it set to the center of thickness of the solution film. The obtained spectrum was processed in the same way.

The transmission absorption spectrum was measured at the same position of the same particle without changing the optics except removing the notch filter. The built-in halogen lamp was used as light source for the absorption measurement. The baseline was confirmed at nearby the particle. However, obtained spectrum was deformed and baseline-drifted due mostly to scattering through the particle. The baseline drift was corrected by subtracting the offset with the linear extrapolation of the baseline (Fig. S3). The obtained absorbance (0.02–0.08) at the excitation wavelength (532 nm, near the peak) was used for the UC-QY calculation.

At the wavelength (532 nm), the error caused by subtraction of baseline was smaller than the shorter wavelength because the wavelength range used to determine the level of the baseline (550-590 nm) was just 20-30 nm away from it and the baseline drift was gradual compared to the wavelength distance. The baseline drift became steeper as decreasing the wavelength, so the baseline subtraction with the linear extrapolation tend to give overestimation in absorbance A_S, which gives under estimation of Φ_S through Eq. S9, rather than over estimation. The error was estimated to be less than 10% by compared to the spectral shape of the PtOEP in solution (DMSO and acetone).

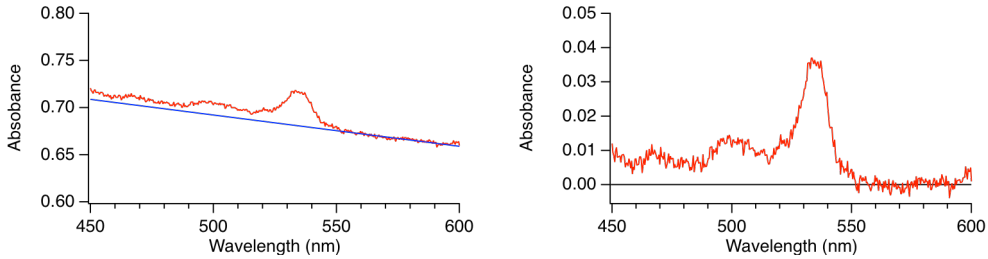

Fig. S3. Left: a typical absorption spectrum of the crystalline particle of PtOEP:C7-sDPA as measured. The line is the extrapolation of the base line for the subtraction of scattering. Right: the same spectrum after subtraction of the scattering.

Generally speaking, the correction with refractive index gives large influence on the result as seen in eq. S9, which was developed for solution sample. This is due to the change in the solid angle of detection with different refractive index of solvent.[1, 9] In the current experiment, the sample was crystalline particle surrounded by the medium (air or Ar). If the emitting volume in the particle is assumed as a point light source, then the effect is the same as for the solution; thus, the refractive index of the medium (i.e. air and Ar, so $n \approx 1$) surrounding the particle can be used for the correction. However, scattering from the inside and at the surface of the particle may affect the solid angle of detection. The estimation of this effect is difficult because the scattering condition depends on the particle. Thus, we used immersion oil (n = 1.404) to check the influence of this effect. The refractive index of the particle must be higher than that of the oil; nevertheless, the difference can be reduced much compared to gaseous medium. Matching of refractive index reduces the scattering. The resulting UC-QY was found to show no significant difference among the media (air, Ar, and the immersion oil) as shown in Fig. 2b in the main text, suggesting that the effect is smaller than expected.

S10. Preparation of the PtOEP-nanocrystal dispersed aqueous solution by the precipitation method

PtOEP solution in spectroscopic grade DMSO (47.2 μM) of 0.2 ml was poured into the 10 ml of distilled water with strong stirring by using a microsyringe. The solution was kept stirring for 30 min under ambient environment. No sediment was observed by naked eye in the obtained reddish purple solution. The absorption spectrum was recorded with a spectrophotometer (*Shimadzu UV3150*).

S11. High-resolution microscopic spectrograph.

The high-resolution microspectroscopic measurements were performed using an inverted fluorescence microscope (Olympus, IX71) equipped with a high N.A. objective lens (Olympus, x 100, N.A. = 1.3). Excitation was provided in an epi-illumination configuration with a CW diode-pumped solid-state 532 nm green laser with an output attenuated by ND filters. The emission was collected by the same objective, passed through a dichroic mirror (532 nm, Semrock) and a notch filter (532 nm, Semrock), and was split into two channels in an image splitter (Optosplit II, Cairn) by another dichroic mirror (532 nm). A short-pass filter (480 nm, Semrock) was used to select the upconverted delayed fluorescence in the first channel while a long-pass filter (590 nm, Nikon) was used in the second channel to detect possible phosphorescence from the absorber molecules. Both channels were imaged side-by-side onto an electron multiplying charge-coupled device (EM-CCD) camera (Andor technology, iXonEM+). For spectroscopic measurements, the image splitter was replaced with an imaging spectrograph (Bunkoukeiki CPL-50LD). The transmission images were taken with a standard tungsten lamp.

S12. The UC-QY measurement using an integration sphere

The UC-QY of PtOEP:DPA crystalline particles was also measured using a specially built setup based on an absolute photoluminescence quantum yield measurement system (*Hamamatsu Photonics C9920-02G*). A short-pass filter (480 nm) was inserted between an integration sphere and a photonic multichannel analyzer (*Hamamatsu Photonics C10027-01*). The sensitivity of the analyzer in the 250-950 nm range before and after the insertion of the short-pass filter was corrected using deuterium and halogen standard light sources.[10] The quality of the integrating sphere in the absence of the short-pass filter was checked using degassed anthracene solution in ethanol (50 μM). The photoluminescence QY of the solution was comparable to the previous report.[10, 11] It was confirmed that photoluminescence QY has not changed at 415-480 nm by the insertion of the short-pass filter using aerated DPA solution in tetrahydrofuran (0.2 mM) and 405 nm laser (*B&W TEK, BWB-405-40-E*) as an excitation. A collimated top hat shaped excitation light at 532 nm (*Changchun New Industries Optoelectronics Tech. Co. Ltd TDG532-500*) with a diameter of 1.0 mm was introduced into the integration sphere

at the power of 3.0 W/cm^2. Photon numbers in the 250-950 nm range were measured in the presence and the absence of the sample under the excitation. The emission QY (Φ_{em}) was determined using the following equation: [10]

$$\Phi_{em} = \frac{PN(\mathrm{Em})}{PN(\mathrm{Abs})} = \frac{\int \frac{\lambda_{em}}{hc}\left[I_{em}^{S}(\lambda_{em}) - I_{em}^{R}(\lambda_{em})\right] d\lambda_{em}}{\int \frac{\lambda_{ex}}{hc}\left[I_{ex}^{R}(\lambda_{ex}) - I_{ex}^{S}(\lambda_{ex})\right] d\lambda_{ex}}, \qquad \text{(S10)}$$

where PN(Abs) is the number of photons absorbed by the sample, PN(Em) is the number of photons emitted from the sample, λ_{em} is the emission wavelength, and λ_{ex} is the excitation wavelength, h is Planck's constant, c is the velocity of light, I_{ex}^{S} and I_{ex}^{R} are the integrated intensities of the excitation light in the presence and the absence of the sample, respectively, and I_{em}^{S} and I_{em}^{R} are the integrated emission intensities in the presence and the absence of the sample, respectively. In the integration processes of the excitation and emission intensities, 415 nm < λ_{em} < 480 nm and 522 nm < λ_{ex} < 543 nm were selected to determine the value of Φ_{em}. Finally, the UC-QY was obtained by doubling the emission QY as $\Phi_{UC} = 2\Phi_{em}$ to express full conversion as unity because $\Phi_{em} = 0.5$ is the full conversion in the UC process where two excitation photons generate one emission photon.

S13. Transmission electron microscope (TEM) observation

Transmission electron microscopy (TEM) and high-angle annular dark field imaging in scanning transmission electron microscopy (HAADF/STEM) were performed to examine the morphology of the cross section of the PtOEP:C7-sDPA particles (Fig. 4). HAADF/STEM analysis involves measurement of electrons scattered at high angles from the incident beam with an annular dark-field detector in STEM.[12] In this technique, the intensity of the image is related to the atomic number Z of the atoms responsible for the scattering. This technique is routinely used to investigate compositional structures and boundary segregations on bulk materials.[13] This method can provide more information than scanning electron microscopy (SEM) with energy dispersive X-ray spectroscopy or electron probe X-ray microanalyzer, especially for samples with low atomic concentrations. The samples within the light-cured resin were cut into thin sections up to 100 nm thick with a diamond knife on an ultramicrotome

(Ultracut UCT, Leica). The specimens were mounted on a cupper TEM grid, made electrically conductive by coating with a thin carbon film according to the conventional method, and inserted into a TEM specimen holder. TEM and HAADF/STEM images were obtained with a Tecnai Osiris (FEI, USA), operating at 200 kV.

Supplemental Data

S14. Absorption and emission spectra of the compounds used

For the solution samples, the data were recorded with a *Shimadzu UV3150* spectrophotometer for absorption and with a spectrofluorimeter (*Hitachi F-4500*) for emission. For the powder samples, recorded with an *OceanOptics USB2000-FLG* spectrometer.

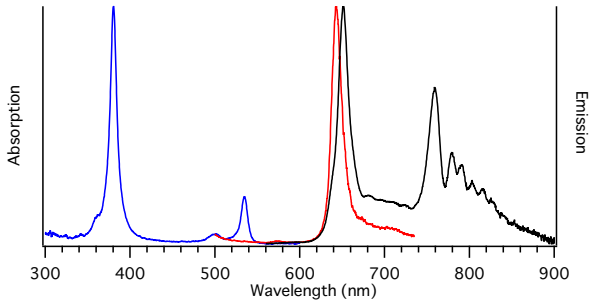

Fig. S4. Absorption (blue) and emission (red) spectra of PtOEP in THF, and the emission spectrum of PtOEP powder (black).

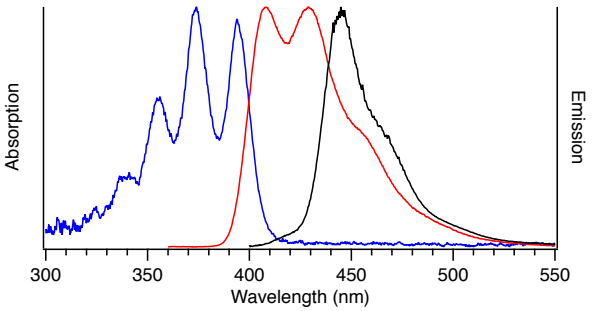

Fig. S5. Absorption (blue) and emission (red) spectra of DPA in THF, and the emission spectrum of DPA powder (black).

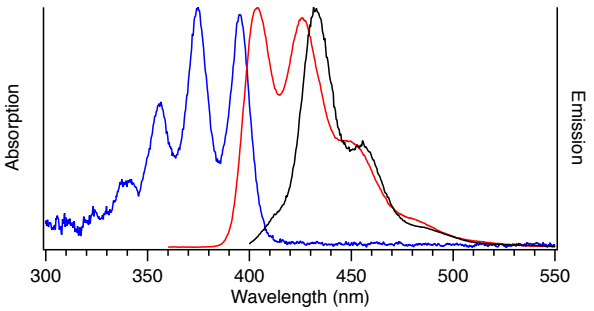

Fig. S6. Absorption (blue) and emission (red) spectra of C7-sDPA in THF, and the emission spectrum of C7-sDPA powder (black).

S15. Polarized microscope observation of PtOEP:DPA cast sample

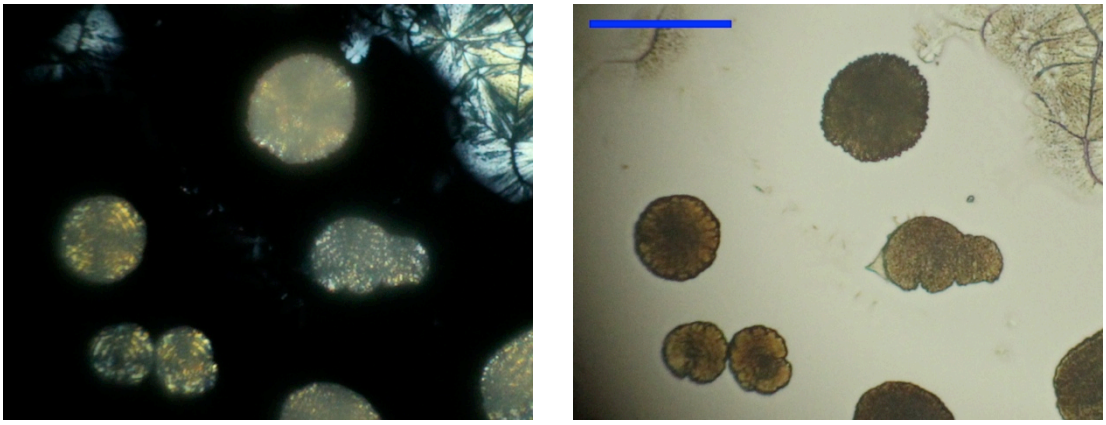

Fig. S7. Polarized (left) and non-polarized (right) transmission microscopic image of the cast sample of PtOEP:DPA from the THF-mixed solution. The scale bar is 50 μm.

S16. SEM image of crystalline particle of PtOEP:DPA

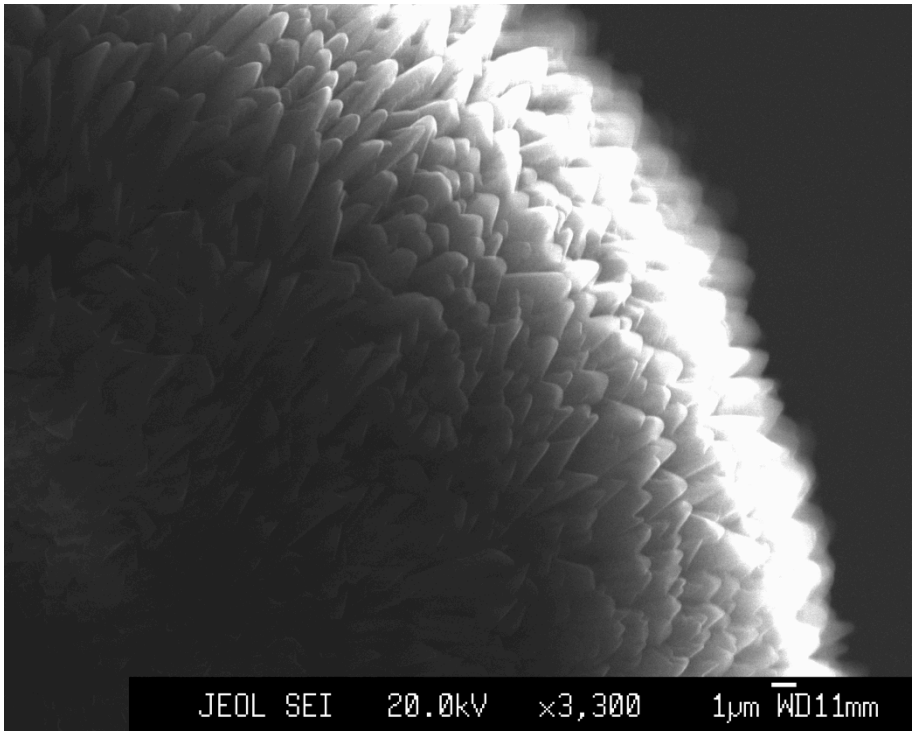

Fig. S8. Scanning electron microscopic image of a round crystalline particle of PtOEP:DPA.

S17. UC emission decay and the triplet lifetime

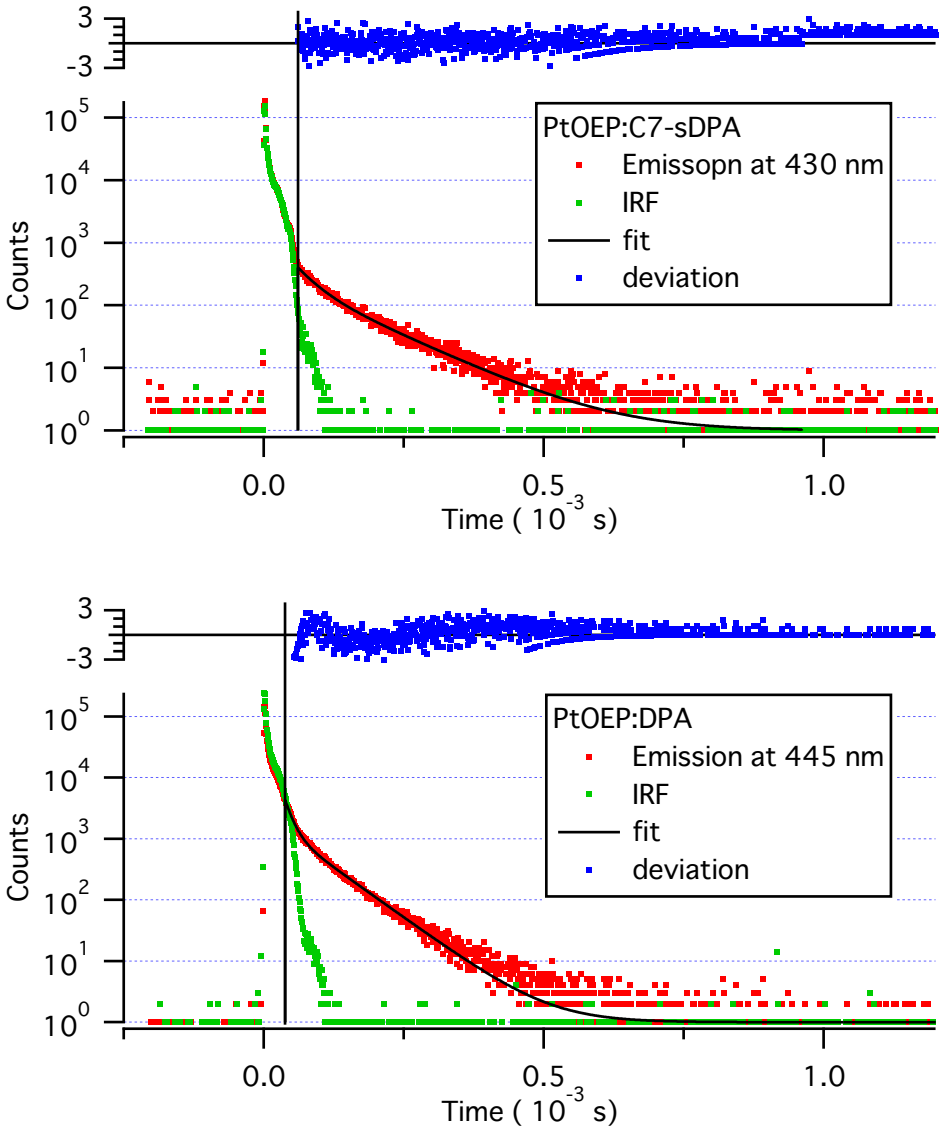

Fig. S9. UC emission lifetimes of PtOEP:C7-sDPA (upper) and PtOEP:DPA (lower) excited at 532 nm. The non-variant part of the decay by changing the excitation intensity was analyzed with biexponential function. The obtained lifetimes are τ_1 = 31 μs (a_1 = 77 %) and τ_2 = 110 μs (a_2 = 23 %), giving an average lifetime, $\langle\tau\rangle = \left(a_1\tau_1^2 + a_2\tau_2^2\right)/\left(a_1\tau_1 + a_2\tau_2\right)$, of 69 μs for C7-sDPA and τ_1 = 13 μs (a_1 = 93 %) and τ_2 = 66 μs (a_2 = 7 %), giving weighted average of $\langle\tau\rangle$ = 27 μs for DPA. The estimated triplet lifetime τ_{TE} was obtained to be 140 μs for C7-sDPA and 54 μs for DPA from the relation as $\tau_{TE} = 2\langle\tau\rangle$.

S18. Data of excitation-intensity dependence of the UC emission

1. PtOEP:DPA

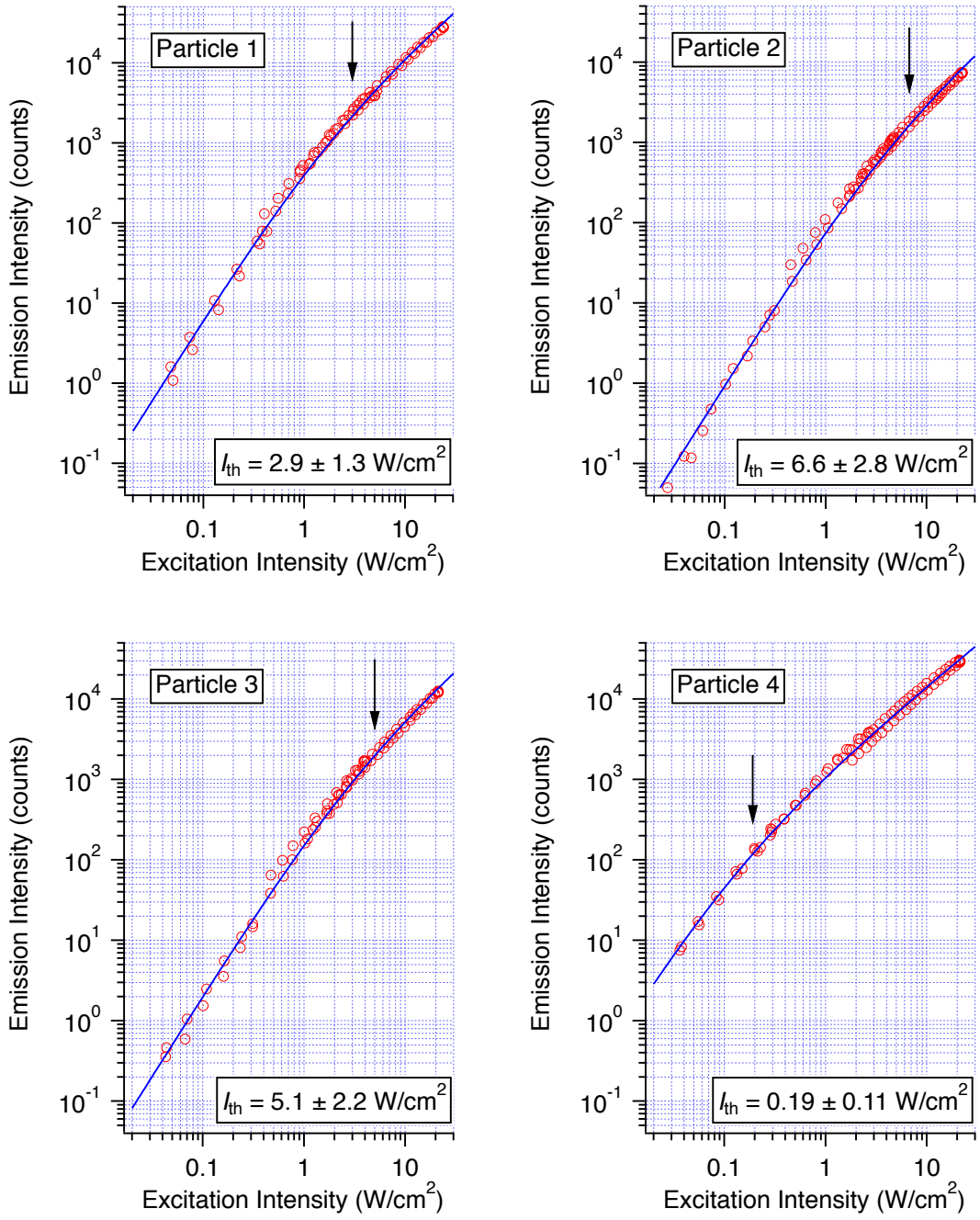

Fig. S10. The excitation intensity dependence of the UC emission at 440 nm of PtOEP:DPA individual crystalline particles (Particle 1-4, circles) with the curve fit with Equation 1. The threshold intensities (I_{th}) were obtained from the curve fits. The arrows show the approximate position of the I_{th}'s.

2. PtOEP:C7-sDPA

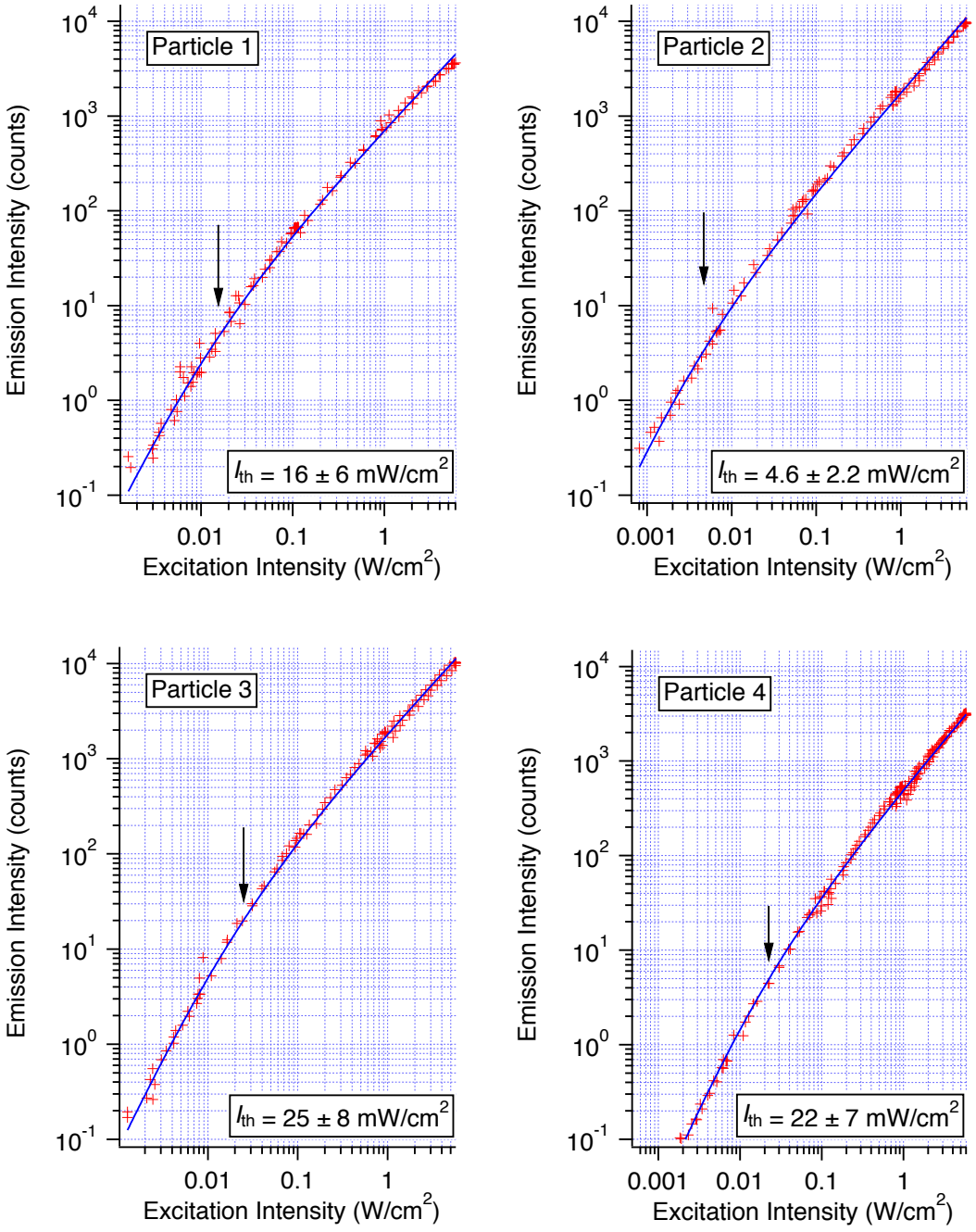

Fig. S11. The excitation intensity dependence of the UC emission at 440 nm of PtOEP:C7-sDPA individual crystalline particles (Particle 1-4, crosses) with the curve fit with Equation 1. The threshold intensities (I_{th}) were obtained from the curve fits. The arrows show the approximate position of the I_{th}'s.

S19. UC quantum yield of the PtOEP:C7-sDPA sample with the molar ratio of 1:1000

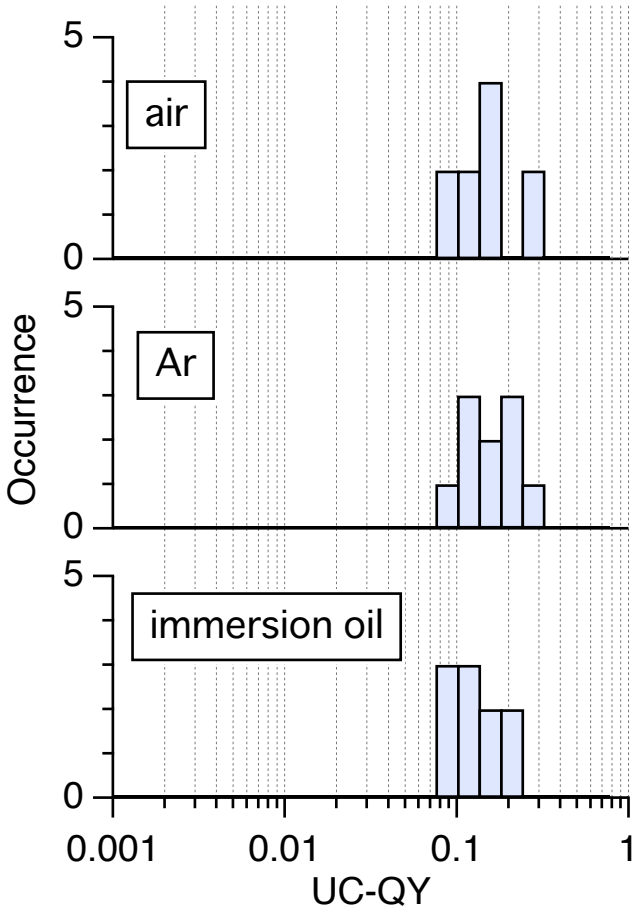

Fig. S12. Histogram of the upconversion quantum yield (UC-QY) of ten individual microparticles of PtOEP:C7-sDPA with the molar ratio of [PtOEP]:[C7-sDPA]=1:1000 in different environments.

References

1. Y. Murakami, *Chem. Phys. Lett.*, 2011, **516**, 56-61.
2. A. Monguzzi, J. Mezyk, F. Scotognella, R. Tubino and F. Meinardi, *Phys. Rev. B*, 2008, **78**, 195112.
3. A. Monguzzi, R. Tubino, S. Hoseinkhani, M. Campione and F. Meinardi, *Phys. Chem. Chem. Phys.*, 2012, **14**, 4322-4332.
4. P. Duan, N. Yanai and N. Kimizuka, *J. Am. Chem. Soc.*, 2013, **135**, 19056-19059.
5. Y. Fujiwara, R. Ozawa, D. Onuma, K. Suzuki, K. Yoza and K. Kobayashi, *J. Org. Chem.*, 2013, **78**, 2206-2212.
6. A. E. Siegman, *Lasers*, Oxford University Press, Oxford, 1986.
7. T. Karstens and K. Kobs, *J. Phys. Chem.*, 1980, **84**, 1871-1872.
8. C. Würth, C. Lochmann, M. Spieles, J. Pauli, K. Hoffmann, T. Schüttrigkeit, T. Franzl and U. Resch-Genger, *Appl. Spectroscop.*, 2010, **64**, 733-741.
9. J. R. Lakowicz, *Princeples of Fluorecence Spectroscopy, 3rd. Ed.*, Sptinger, N.Y., 2006.
10. K. Suzuki, A. Kobayashi, S. Kaneko, K. Takehira, T. Yoshihara, H. Ishida, Y. Shiina, S. Oishi and S. Tobita, *Phys. Chem. Chem. Phys.*, 2009, **11**, 9850-9860.
11. W. H. Melhuish, *J. Phys. Chem.*, 1961, **65**, 229-235.
12. D. E. Jesson and S. J. Pennycook, *Proc. R. Soc. Lond. A* 1993, **441**, 261.
13. J. H. Laurer and K. I. Winey, *Macromlecules*, 1998, **31**, 9106–9108.